Single Motor-Controlled Mechanically Reconfigurable Reflectarray

Zhongyao Cao, Yue Li, *Senior Member, IEEE*, Zhijun Zhang, *Fellow, IEEE*, and Magdy F. Iskander, *Life Fellow, IEEE*

***Abstract*— In this article, a mechanically reconfigurable 1-D reflectarray actuated by a single motor is proposed. The elements are designed as metal tubes that are lifted by the ejectors. To achieve continuous phase growth in a limited space, the discontinuity of the Archimedean spiral is utilized. Then, a novel drive mechanism is constructed to transfer the power of the motor to each element. The combination of the Archimedean spiral cam and the follower effectively converts the rotation of the shafts to the linear motion of the element. In conjunction with the timing pulleys and timing belts, the Archimedean spiral cams generate a periodic changing phase gradient over time. The whole structure is supported by low-cost acrylic plates with fasteners. The main parts are composed of standard components and the overall structure is easy to realize. The reflectarray at normal incidence offers a beam steering range from −60° to 60° in one dimension at 5 GHz. The beam coverage test demonstrates a maximum improvement in the received signal level of 16 dB in the multipath environment. This work provides a new solution to the design of mechanically reconfigurable reflectarrays.**

***Index Terms*— Archimedean spiral cam, drive mechanism, reconfigurable reflectarray, timing belts, timing pulleys.**

I. Introduction

As THE user density increases, the signal coverage of wireless communication has increasingly become a challenging problem. The number of base stations deployed in the city is increasing, which leads to large energy loss. Besides, in the urban environment, the radio waves from the base station are usually blocked by the buildings and walls. The so-called blind spots are formed and the quality of communication deteriorates seriously. Deploying passive repeaters has been proven as an efficient way to cover the blocked areas [1]. When the direct line-of-sight (LOS) path is blocked, the repeaters reradiate the received power and offer an additional path to the users.

In recent years, passive repeaters with a fixed beam angle have been widely studied for improving wireless communication environment. The reflectarray with the preset phase on the aperture is a good substitute. The wave illuminating the reflectarray can be redirected to the required angle ranging from 50° to 90° [2], [3], [4], [5], [6], [7]. A corner reflectarray achieves the beam steering of wireless signals at 90° [8]. Dual-antenna system composed of both receiving and transmitting antennas is proposed [9], [10], [11]. It transfers the received energy to the transmitting antenna by the power combiner. The dual-antenna systems comprising a four-element folded-patch antenna array and an open-ended waveguide are combined to provide flexible beam control [9]. Dual-antenna systems consisting of planar Yagi-Uda antennas are proposed to redirect the energy to the endfire direction [10]. The improvement of dual-antenna systems on MIMO performance is demonstrated in [11].

Compared with the passive repeaters with a fixed beam, reconfigurable repeaters allow a larger coverage area. Especially for the repeaters with a large aperture, the focused narrow beam only covers a limited range. Therefore, the demand for the reconfigurable capability of the passive repeaters is proposed. The reconfigurable passive repeater should be able to steer the beam to the users in blind areas. The reconfigurability methods of the reflectarray can be sorted into two categories. A commonly used method is to electrically control the phase using p-i-n diodes [12], [13], [14], microelectromechanical systems (MEMS) switches [15], [16], [17], varactors [18], [19], and liquid crystal [20]. However, the aperture efficiency is limited by the element loss and quantization loss. Besides, the bias circuits and corresponding control system are required.

The other method is to mechanically control the phase of each element [21], [22], [23], [24], [25], [26], [27]. The orientation or height of the element can be precisely controlled by actuators. Accordingly, the phase of each element can be reconfigured dynamically. For circularly polarized reflectarrays, micromotors are used to rotate the elements and a phase shift range of 360° can be achieved [21]. For linearly polarized reflectarrays, the height of each element [22] is adjusted by the actuators to achieve beam steering. However, the actuators used in the reflectarrays need to be controlled individually by the field-programmable gate arrays (FPGAs) and microcontroller unit (MCU). The control circuit will be complicated when continuous beam scanning is required. Deformable ground is introduced in [25], which reduces the number of actuators to four. As a simplified control scheme, the single motor-controlled design is of interest. The reflectarray based

Manuscript received 17 July 2022; revised 6 October 2022; accepted 17 October 2022. Date of publication 14 November 2022; date of current version 19 January 2023. This work was supported by the National Natural Science Foundation of China under Contract 61971254 and Contract 62271279. *(Corresponding author: Zhijun Zhang.)*

Zhongyao Cao, Yue Li, and Zhijun Zhang are with the Department of Electronic Engineering, Tsinghua University, Beijing 100084, China, and also with the Beijing National Research Center for Information Science and Technology, Tsinghua University, Beijing 100084, China (e-mail: zjzh@tsinghua.edu.cn).

Magdy F. Iskander is with the Hawaii Center for Advanced Communications, University of Hawai'i at Manoa, Honolulu, HI 96822 USA (e-mail: magdy.iskander@gmail.com).

Color versions of one or more figures in this article are available at https://doi.org/10.1109/TAP.2022.3221036.

Digital Object Identifier 10.1109/TAP.2022.3221036

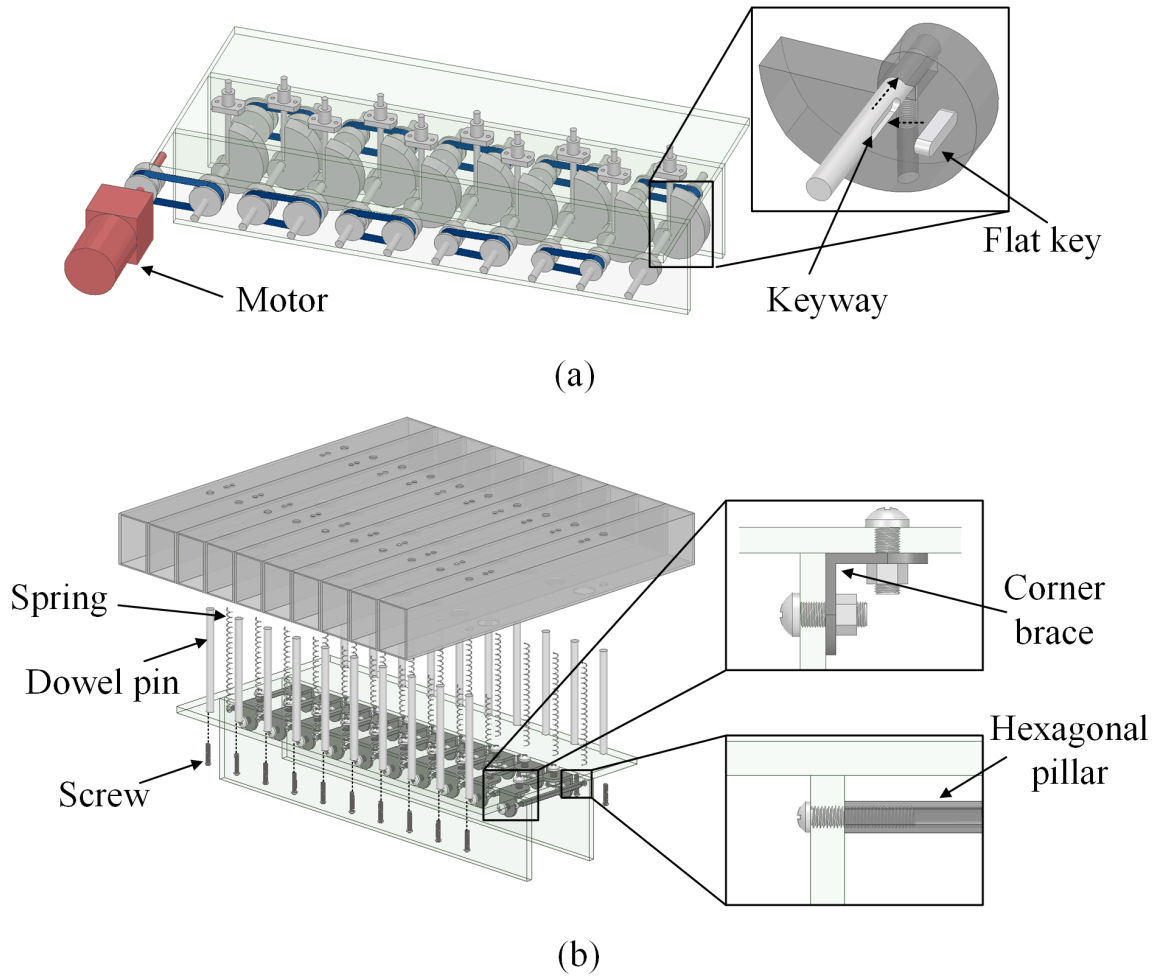

Fig. 1. Configuration of the mechanical reconfigurable reflectarray. (a) Drive mechanism and Archimedean spiral cam of the reflectarray. (b) Supporting structure of the reflectarray.

on the mechanical rotation of the array is proposed in [26]. In [27], a foldable reflectarray with flexible surfaces can be stretched by a single motor. However, it is still a challenge to achieve a single motor-controlled simple reflectarray with a wide scanning range for wireless communication signal coverage.

In this article, a single motor-controlled mechanically reconfigurable reflectarray is proposed. The elements are composed of metal tubes. To control the reflectarray, a drive mechanism is constructed by using timing pulleys and timing belts. By introducing the Archimedean spiral cam, the change in angle can be transferred into the change in height. Then, the movement of each element can be transmitted by the drive mechanism. The movement process of the transmission structure is periodic, and the reflectarray achieves a periodic beam scanning as the motor keeps driving. The proposed reflectarray achieves a beam steering range of -60° to 60°. To evaluate the performance in the multipath environment, a beam coverage test is conducted. The results show that a maximum improvement in the signal level of 16 dB is achieved. The improvement on different points demonstrates a wide coverage range of the reflectarray.

The remainder of this article is organized as follows. Section II displays and discusses the physical configuration and the movement scheme. The fabrication and radiation performances are presented in Section III. The beam coverage test is illustrated in Section IV. The work is concluded in Section V.

II. Configuration and Movement Scheme of the Reflectarray

A. Overall Structure

Fig. 1 shows the overall configuration of the mechanically reconfigurable reflectarray. The drive mechanism and the Archimedean spiral cams of the reflectarray are shown in Fig. 1(a). The linear bearings are added on top of the cams to achieve linear motion with low friction. It makes the conversion between the rotation of the cam and the linear motion of the ejector rod more stable. A keyway of 3×3 mm^2 is added to both the shaft and the cam. Stable synchronous rotation can be realized with a flat key embedded in the keyway. Screw holes are drilled inside the cam. Installing a jack screw in the hole effectively avoids lateral movement along the shaft. Besides, timing belts combined with timing pulleys are used for power transmission. Screw holes are also prepared on the pulleys and the installation of jack screws locks the pulley on the shaft. By using flat key and jack screws,

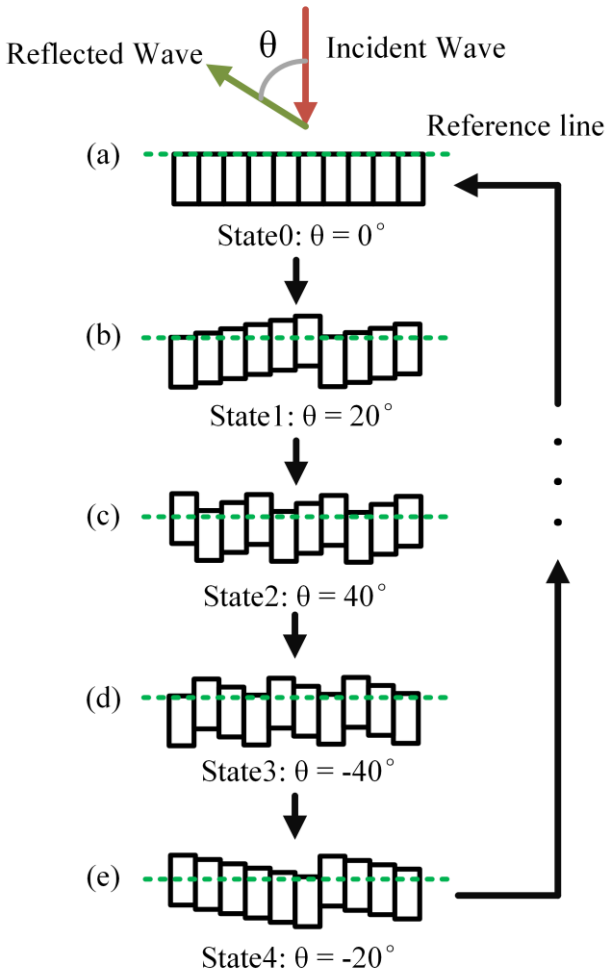

Fig. 2. Element height distribution and beam angle calculated from array factors in (a) state 0, (b) state 1, (c) state 2, (d) state 3, and (e) state 4.

the Archimedean spiral cam, pulley, and shaft can achieve synchronous rotation.

As displayed in Fig. 1(b), the elements and drive mechanism are supported by three pieces of acrylic plates with a thickness of 5 mm. We utilize standard fasteners to connect the acrylic plates and form the supporting structure. Corner braces with screws and nuts are used to connect the top and side plates. Internally threaded hexagonal copper pillars and screws are combined to reinforce two side plates. To reduce the weight of the structure, the elements are designed as hollow rectangular metal tubes. For each tube, we fix two dowel pins on the top plate with screws. The dowel pins pass through the holes in the element and act as a guide rail. It guarantees that the element moves up and down in a straight line. Furthermore, each element is held by two springs with hooks. The springs ensure that the elements can be reset to the reference line in any arrangement.

B. Movement Scheme

In the beginning, to clearly illustrate the movement process, the distributions of the elements in five particular states in a period are shown in Fig. 2. Ten metal tubes with a width of $\lambda/2$ are used as the elements of the reflectarray. To achieve beam scanning, an adjustable phase distribution should be implemented on the aperture of the reflectarray. The reflection phase of each element can be controlled by changing the distance that the wave travels. Then, a specific phase distribution can be achieved by arranging the elements at different heights.

A model describing the movement of the elements is presented to help understand how the array is reconfigured

$$h_j = v_j t \tag{1}$$

$$v_{j+1} = v_j + \Delta v \tag{2}$$

$$\alpha_j = 2h_j k_0 \tag{3}$$

$$\text{If} \quad h_j > \frac{\lambda}{2}, \quad h_j = h_j - \frac{\lambda}{2}, \quad j = 1, \ldots, n \tag{4}$$

where v_j is the rising velocity of the elements and h_j is the height of the jth element from the reference line. α_j is the reflection phase of the jth element, n represents the number of elements in the reflectarray, and Δv is a constant.

In the proposed movement scheme, the jth element rises at a velocity of v_j. The phase of the element is determined by the height h_j. We reset the height of the element h_j to zero when h_j reaches $\lambda/2$. The velocity of the $(j+1)$th element is Δv faster than that of the jth element. Since the velocity difference between the adjacent elements is constant, an equal phase step between any two adjacent elements is guaranteed. Then, a uniform phase gradient can be generated on the aperture.

In Fig. 2, the five states are presented in chronological order. In state 0, all the blocks are arranged on the reference line, as shown in Fig. 2(a). Some elements have been reset to the reference line in state 1 with the beam steered to 20°. In state 2, some elements will be reset multiple times with the beam steered to 40°. As the phase step increases, the beam angle θ continues to increase from 0° to 90°. When the phase step between elements exceeds 180°, the beam turns to the other half of the plane and decreases from −90° to 0°. Finally, the phase difference reaches 360° and the reflectarray recovers to the original state. A new period starts from state 0. Therefore, the proposed reconfigurable reflectarray can perform a periodic movement. The beam covers the range from −90° to 90° in a period.

C. Archimedean Spiral Cam

Traditionally, to achieve beam steering, large phase variation is required. Accordingly, the height of each element will vary a lot and the reflectarray will take up a large space. To tackle this problem, the structure of an Archimedean spiral cam with a follower is utilized. Fig. 3 displays the combined mechanical structure. The mechanism allows continuous phase growth in a limited space. The polar coordinate equation of the Archimedean spiral is

$$r = a\varphi + b \tag{5}$$

where a is a coefficient and b is a constant. During the rotation of the cam from 0° to 360°, the follower keeps rising. Once the rotation angle exceeds 360°, the follower falls back to the starting point and starts a new cycle. If we set the coefficient

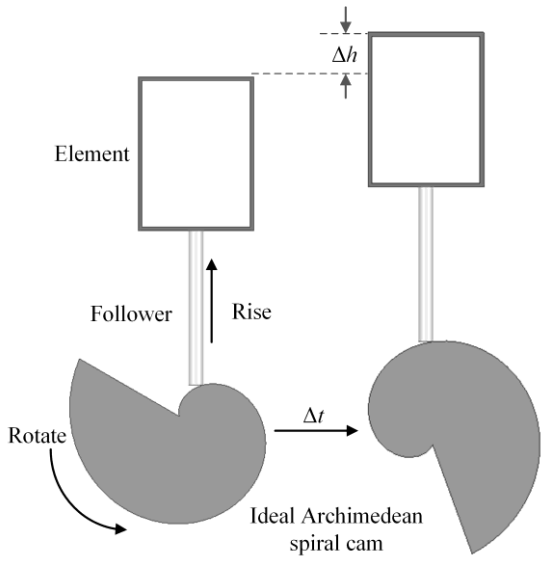

Fig. 3. Two states picked from the rotation process of the ideal Archimedean spiral cam.

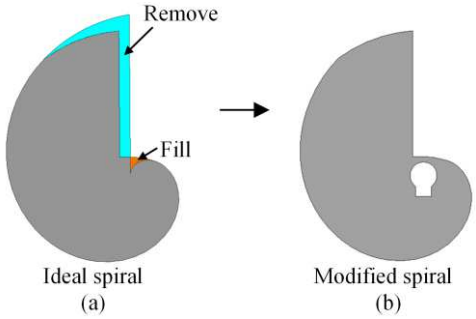

Fig. 4. Modification process of the Archimedean spiral cam. (a) Original structure. (b) Modified structure.

$a = \lambda/4\pi$, the height difference will be equal to $\lambda/2$, which corresponds to a phase difference of 360°. Therefore, the phase continues to increase when crossing the discontinuity, and the height variation is limited to $\lambda/2$.

When we set $a = \lambda/4\pi$, r will always be b larger than $\lambda/2$ at the angle of $\varphi = 360°$. Since the distance between elements is $\lambda/2$, the Archimedean spiral cams will conflict with the shafts. Therefore, the maximum value of the spiral should be reduced and a modification is demanded. The process is displayed in Fig. 4. The blue part of the Archimedean spiral cam is removed and the spiral curve is replaced by an arc with a diameter of 27 mm. The maximum axial distance is reduced to the radius of the arc. Then, a rectangular area with a width of 2 mm is removed to reduce phase error caused by the radius of the follower. The constant b of the modified spiral is set to 0.5 mm. Therefore, to allow space for a keyway and a round hole in the cam as shown in Fig. 4(b), the yellow part picked from an ellipse shown in Fig. 4(a) is united with the Archimedean spiral. The length of the major axis of the ellipse is 7.2 mm and the length of the minor axis is 3.6 mm.

It must be mentioned that the modification of the cam causes phase error. The error emerges at a narrow range during the rotation of the cam and the maximum phase error is 37.2°. To avoid the modification of the cam, the distance between adjacent shafts should be increased. When setting adjacent shafts at different heights, the distance will be larger than $\lambda/2$. This kind of arrangement can avoid modification and phase errors. In this design, to verify the feasibility of the structure, we simply set the shafts at the same height.

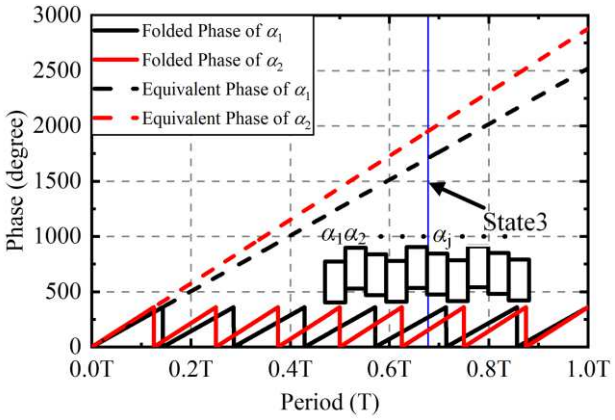

Fig. 5. Phase variation of the first two elements in a period.

Fig. 5 shows the phase variations of the first two elements of the reflectarray. The equivalent phase of the two elements keeps increasing linearly. After introducing the Archimedean spiral cam, the phase curve can be folded in a unit of 360°. The folded phase is equivalent to the demanded one, but the height variation is limited to $\lambda/2$. When the phase step reaches 360° at T, the two elements recover to the same height and a new period starts.

D. Drive Mechanism

According to (2), a constant velocity difference between any two adjacent elements is required. Using a large number of motors and the corresponding velocity control devices to achieve this relationship complicates the system. Therefore, a novel drive mechanism is proposed to implement the movement scheme with only one motor. The drive mechanism is capable of transmitting the power from the motor to all the elements. By using timing pulleys with different diameters, the angular velocity ratio between the elements can be adjusted proportionally. Another significant function of the Archimedean spiral cam is to convert rotation to linear motion. According to the equation of the Archimedean spiral (5), the constraint of linear velocity (2) can be converted into the constraint of angular velocity on the shaft

$$\omega_{j+1} = \omega_j + \Delta\omega \tag{6}$$

where ω_j is the angular velocity of the jth shaft and $\Delta\omega$ is a constant.

Then, we only need to use the drive mechanism to achieve such an angular velocity relationship for all the elements. For a set of timing pulleys linked by a timing belt, the linear velocities of all the pulleys are always the same. Thus, the angular velocity is inversely proportional to the number of

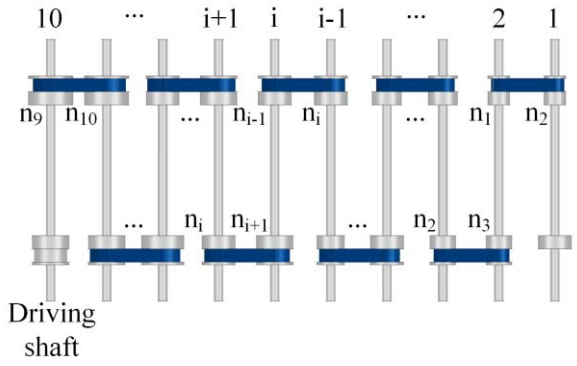

Fig. 6. Connection relationship between the timing belts and the timing pulleys.

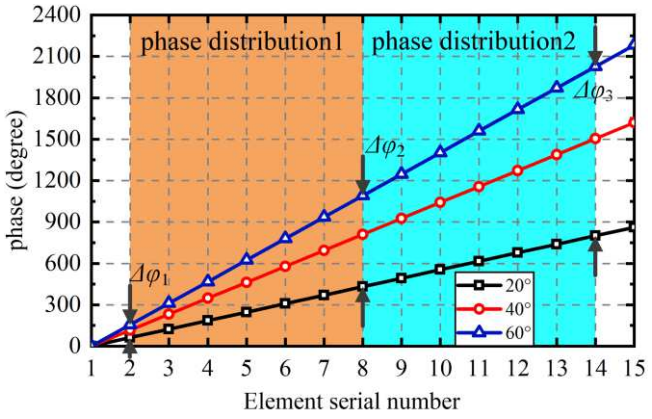

Fig. 7. Demanded phase distribution of the elements on the aperture for the beam steered to 20°, 40°, and 60°.

cogs on the timing pulleys. To satisfy the constraint in (6), a drive mechanism with alternately arranged timing belts is proposed.

The connection relationship between the timing pulleys and the timing belts is presented in Fig. 6. The number of cogs on the ith timing pulley is n_i. For this type of arrangement, the ratio of angular velocity between the ith and $(i-1)$th shaft satisfies

$$\frac{\omega_i}{\omega_{i-1}} = \frac{n_i}{n_{i-1}}. \tag{7}$$

By taking the value of i from 1 to n in (7), the relationship between the angular velocities of the shafts and the number of cogs can be obtained

$$\omega_1 : \omega_2 : \cdots : \omega_n = n_1 : n_2 : \cdots : n_n. \tag{8}$$

Then, the constraint of angular velocity in (6) can be converted into the constraint of the number of cogs on the timing pulleys

$$n_{i+1} = n_i + \Delta n \tag{9}$$

where Δn is a constant. Therefore, we only need to select specific timing pulleys to satisfy the arithmetic relationship of the number of cogs.

However, considering the physical implementation, the feasible phase distribution on the aperture of the mechanically reconfigurable reflectarray is different from that of the electrically reconfigurable reflectarray. Fig. 7 displays three demanded phase curves for the elements sampled at $\lambda/2$ intervals on the aperture when the beam is steered to 20°, 40°, and 60°. Phase distribution 1 is traditionally utilized on the electrically reconfigurable reflectarray. As the beam scans, the phase variation ratio of each element is not critical for electrical phase control. However, for mechanical phase control, the phase variation in distribution 1 with a large ratio of 1:7 between $\Delta\varphi_1$ and $\Delta\varphi_2$ is hard to implement. The phase variation ratio means that a large velocity ratio is demanded. If a larger aperture is to be achieved, an exaggerated velocity ratio is required, which is difficult to achieve with a mechanical structure. By contrast, phase distribution 2 will be a good solution to the problem. It has the same beam angle but a much lower phase ratio of only 7:13 between $\Delta\varphi_2$ and $\Delta\varphi_3$. In addition, the phase error is determined by the ratio of the angle with error on the cam to the entire circumference. On average, when using the same cam, the phase error is the same under both phase distributions.

In the drive mechanism of the reflectarray, we set n_1 equal to 14 and Δn equal to 2. Then, we can get a set of elements with the linear velocity satisfying $v_1{:}v_2{:}\cdots{:}v_n = 7:8{:}\cdots{:}n+6$. In addition, we need to calculate the suitable length of the timing belt by the center distance and the diameters of the timing pulleys in a set. When the belt is tightened, the theoretical length of the timing belt is expressed as

$$L = 2a + \frac{(d_1+d_2)\pi}{2} + \frac{(d_1-d_2)^2}{4a} \tag{10}$$

where a is the center distance between two timing pulleys, and d_1 and d_2 are the diameters of the timing pulleys. We choose the MXL-type timing pulleys with a pitch of 2.032 mm. The number of the cogs on the timing pulleys and timing belts in the design are summarized in Table I.

TABLE I
NUMBER OF COGS ON THE TIMING PULLEYS AND TIMING BELTS

Pulley	Number	Belt	Number
n_1	14	N_1	44
n_2	16	N_2	46
n_3	18	N_3	48
n_4	20	N_4	50
n_5	22	N_5	53
n_6	24	N_6	54
n_7	26	N_7	56
n_8	28	N_8	58
n_9	30	N_9	60
n_{10}	32		

III. PROTOTYPE AND RADIATION PERFORMANCE OF THE REFLECTARRAY

A. Simulated Results

The proposed reflectarray is simulated by HFSS 19.0, and Fig. 8 presents the simulated scanning performance at 5 GHz. The elements are set to be perfect electric conductor blocks with a width of 30 mm ($\lambda/2$) and a length of 300 mm (5λ). To demonstrate the performance of the reflectarray under ideal

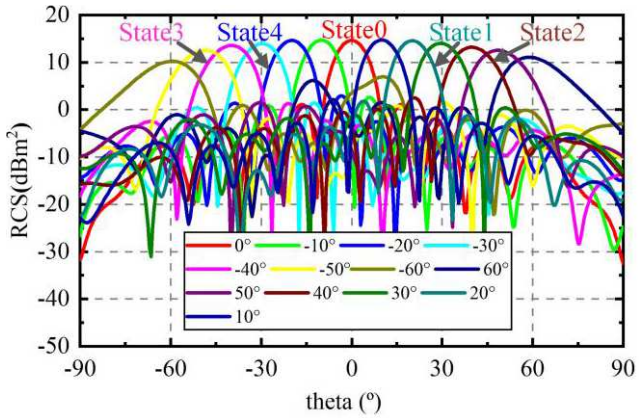

Fig. 8. Simulated scanning performance of the reflectarray with ten elements under normal incidence plane wave.

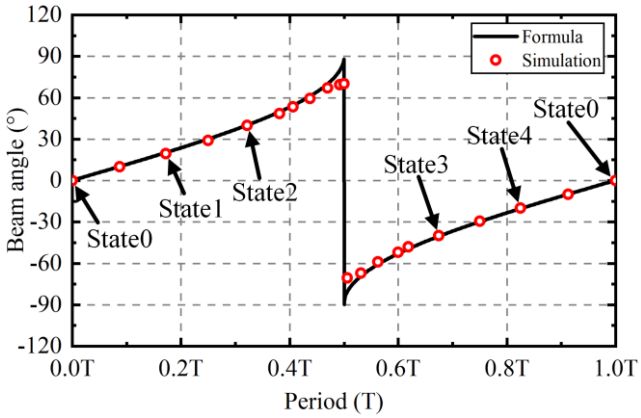

Fig. 9. Variations of the beam angle in a period calculated from the simulated results and formula.

TABLE II
SCANNING PERFORMANCE AT DIFFERENT INCIDENT ANGLES

Incident angle (°)	Scanning range (°)	Maximum RCS (dBm^2)	RCS fluctuation (dB)
0	-60~60	14.7	4.5
-20	-60~60	14.8	5.4
-40	-60~60	13.9	5.0
-60	-60~60	11.5	3.2

conditions, the phase errors are ignored in the simulation. In Fig. 8, the bistatic RCS of the reflectarray with ten elements is obtained under normal incidence. The maximum RCS of 14.7 dBm^2 is realized. The scanning range is from $-60°$ to $60°$. Moreover, the scanning performance of the reflectarray at different incidence angles is summarized in Table II. At large incidence angles, the reflectarray is capable of covering the range of $-60°$ to $60°$, but the maximum RCS decreases due to occlusion and the reduction of the equivalent aperture. Because of the reduction of the maximum RCS, the RCS fluctuation is improved when the incidence angle approaches $-60°$.

If we substitute formulas (1) and (2) into (3), we can calculate the reflection phase for each element. According to the formulas of the antenna array factor, if we define α as the phase difference, d as the element space, and β as the wavenumber in free space, then the steered beam angle is given by

$$\theta = \arcsin\frac{\alpha}{\beta d}. \tag{11}$$

Fig. 9 displays the variations of the beam angle in a period calculated from the simulated results and the formula of the array factor. The five specific states are also marked in the figure. As mentioned above, the beam angle first increases from 0° to 90° and turns from 90° to $-90°$ at half of the period $t = T/2$. Then, the beam gradually decreases to 0° and starts a new period at $t = T$. In the range from $-60°$ to $60°$, the simulated results accord well with the results calculated from the formula. When the beam scans to a wider angle, the simulated results deviate from the predicted results. The severe mutual coupling between the elements is the main reason for this phenomenon. The mutual coupling disturbs the phase distribution on the aperture and shifts the beam direction. Moreover, because of the disturbed phase distribution, the RCS of the directed beam drops rapidly as the angle approaches 90°. However, the movement scheme does provide good beam steering from $-60°$ to $60°$.

B. Prototype and Measured Results

To demonstrate the novel concept of the mechanically reconfigurable reflectarray, a prototype is fabricated, as shown in Fig. 10. Most of the components used in the reflectarray are off-shelf low-cost components. Only the tubes, Archimedean spiral cams, acrylic plates, and shafts are customized components. To reduce the weight, the tubes and cams are all made of aluminum alloy. The cams are processed by computerized numerical control (CNC) machines, while the tubes and shafts are milled. For large-scale processing, the cost of mechanical products can be reduced. Therefore, the overall cost of the mechanically reconfigurable reflectarray can be limited to a low level.

In the design, we choose the standard LMH4UU-type linear bearing with an inner diameter of 4 mm. The chrome-plated hard shafts are mounted in linear bearings as the follower. The high surface hardness of the hard shafts prevents surface scratching when moving up and down in the linear bearing. The Archimedean spiral cams and timing pulleys are fastened in series by the chrome-plated soft shafts to achieve synchronous rotation. The soft shafts with high toughness are suitable for use as the rotation shaft. Due to the limited spacing between the elements, the MXL-type timing pulleys and belts with a small pitch are utilized in the drive mechanism. A reflectarray with ten elements is fabricated and measured. The physical aperture of the reflectarray is 300 × 300 mm. The power of the motor is 9.6 W and the motor torque is 8.6 Kg·cm. In the proposed drive mechanism, the use of timing pulleys and belts introduces additional loss. The efficiency of the drive mechanism is lower than that of a system using N small motors. In general, the transmission efficiency of the timing belts can reach 98%. Therefore, the power consumption of the proposed drive mechanism will not increase significantly.

(a)

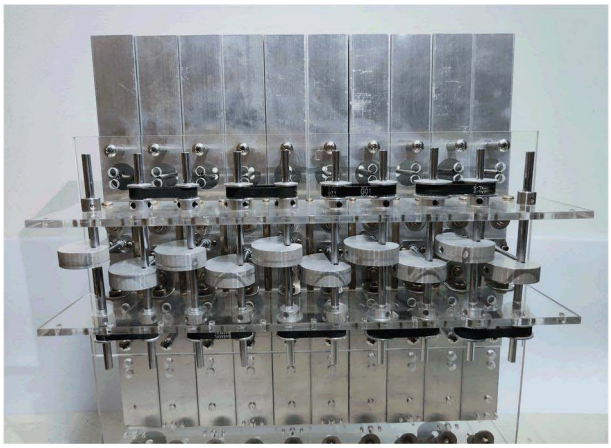

(b)

Fig. 10. Fabricated prototype of the reflectarray. (a) Top view. (b) Bottom view.

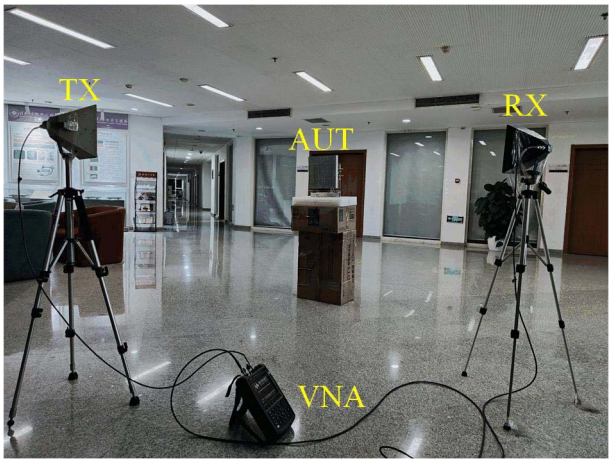

Fig. 11. Bistatic RCS measurement environment of the reflectarray.

The bistatic RCS of the reflectarray is measured in an open hall. The measurement setup is shown in Fig. 11. A cardboard box is used to hold the reflectarray. Two 14 dBi horn antennas are mounted on tripods and placed at a distance of 2 m from the reflectarray. The distance guarantees that the measurement is performed in the far-field region of the horn antennas. The test points are first marked on the floor at intervals of 5°. The center of the semicircle on which the test points locate is at the position of the reflectarray. To guarantee that the horn moves accurately on the semicircle, a plumb is hanged on the bottom of the tripod to align the horn with the test point. The measured $|S_{21}|$ is converted to bistatic RCS. A metal plate inclined at 30° is used for calibration. At $\theta = 0°$, the transmit (TX) and receive (RX) antennas will coincide. Therefore, we set the two horn antennas as close as possible to approximate the results at $\theta = 0°$. Due to the severe mutual coupling between the TX and RX horn antennas, direct coupling contributes a lot to $|S_{21}|$. Therefore, we use the time-domain transform function of the vector network analyzer (VNA) and add a time gate to eliminate undesirable signals.

The measured and simulated bistatic RCS results at 5 GHz are shown in Fig. 12. Three specific states with the beam steered to −30°, −40°, and −50° are displayed. The simulation settings are the same as that in Fig. 8. Beam steering at normal incidence can be observed as the reflectarray changes between different states. Besides, the phase error has a greater impact on the side lobes, but the impact on the main lobes is limited. Although the phase error is not considered in the simulation, the measured results should be consistent with the simulated results in the range of the main lobes. Small deviations are mainly due to fabrication errors and the influence of noises in the measurement environment. In general, there is good agreement between the simulated and measured results.

IV. Beam Coverage Test

To validate the application of the reflectarray, a beam coverage test is made in our laboratory. In practical applications, there are usually transmitters mounted in the corridor. The transmitted signal propagates along the corridor, and the wall brings a loss of more than 20 dB. For lack of path of LOS, the signal level in the laboratory is low. The reflectarray is mounted at the door to improve reception. The users are generally slow-moving or static at a specific site. Then, the reflectarray can steer the beam to cover the user. Signal levels can be improved in a wide range in the laboratory by steering the beam. Fig. 13 presents the measurement setup. A 5 GHz horizontally polarized continuous wave (CW) signal is transmitted in the corridor by the VNA. The signal level is measured by a spectrum analyzer and a dipole probe antenna. Seven points are picked evenly at a distance of 3.6 m. We examine the variation in signal level at these points when beam scanning.

Due to the complex environment inside the laboratory, rays from multiple paths will arrive at the receiver. The received signal is found to exhibit fast fading spatial variation. As the receiver moves in the laboratory, rapid variation of the signal occurs. The signal varies by 20 dB over a distance as small as $\lambda/2$. To demonstrate the enhancement of the signal level at each point reasonably, the received signal is averaged over a distance of 12 cm ($\sim 2\lambda$).

Fig. 14 displays the measured received signal level at seven points from A to G. We in turn steer the beam to the seven test

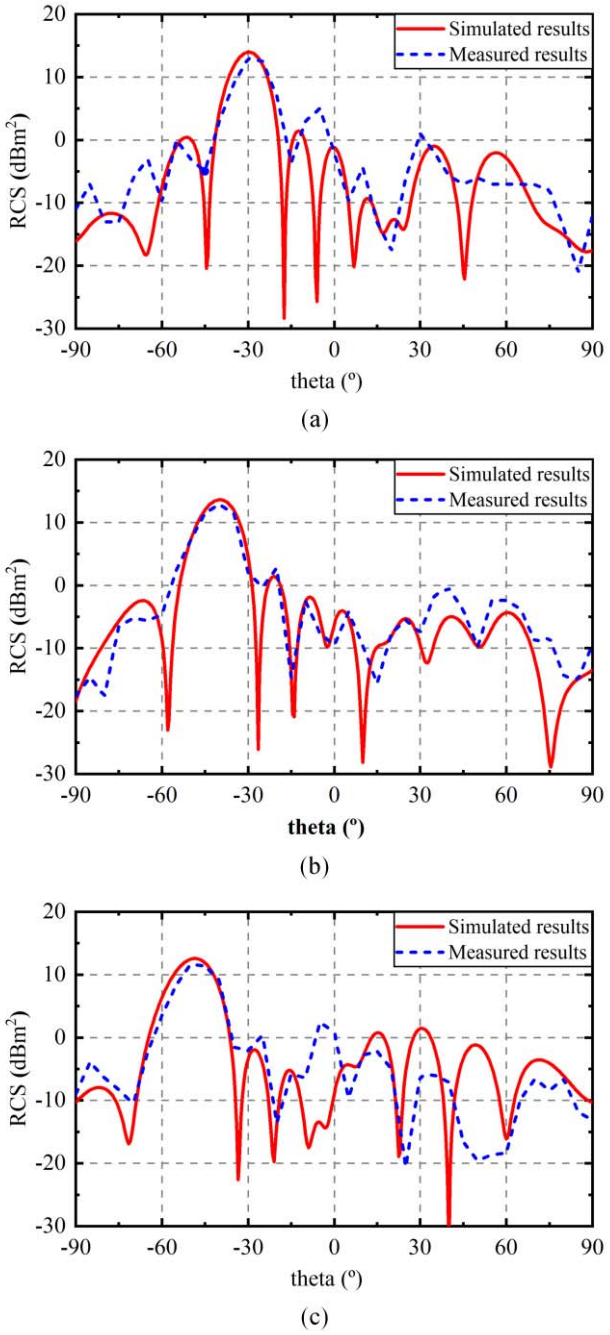

Fig. 12. Measured and simulated bistatic RCS patterns of the reflectarray at 5 GHz at different beam angles. (a) −30°. (b) −40°. (c) −50°.

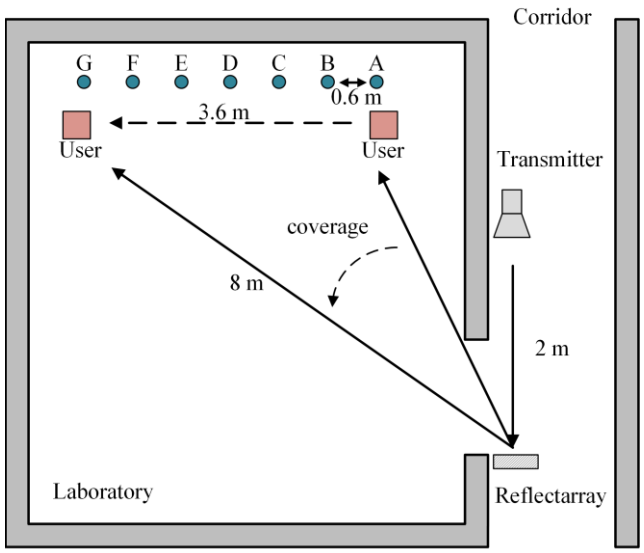

Fig. 13. Beam coverage scenario in the laboratory.

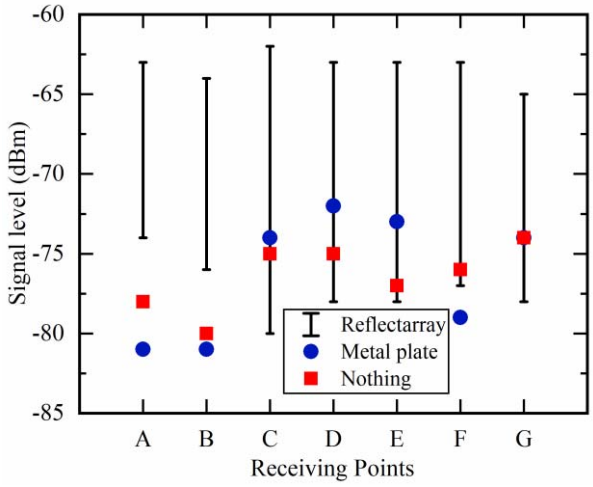

Fig. 14. Measured receiving signal level on seven test points.

points. For each beam, we record the received signal level at all the test points. Therefore, there is a variation in the signal level at each point. As a reference, a metal plate is placed in the same place. Placing the metal plate only achieves limited improvement, and the maximum increment of the signal level is 4 dB. Some points even exhibit signal degradation. After mounting the reflectarray, an obvious improvement can be observed. The signal level increases the most at the point where the beam is directed. An improvement can also be observed on part of the other points that are not aligned by the main beam. From points A to F, the signal level is increased by at least 12 dB. The maximum increment of 16 dB is achieved. Because of the occlusion of the door frame, the maximum signal level on point G is lower than that on other points. Besides, the reflection angle of point G is relatively small. The signal from the transmitter can be reflected by the wall when there is no reflectarray mounted at the door. The reflected ray leads to a high signal level of −74 dBm on point G, but an increment of 9 dB can still be achieved. The results confirm that the reflectarray can effectively improve the signal level in different points of the room when there are no rays in line of sight. A wider range can be covered by the reconfigurable reflectarray compared to the repeaters with a fixed beam angle.

Table III summarizes the performance of this work and other reconfigurable reflectarrays designed for improving the multipath environment. The electric phase controlling [19] has the merits of short response time, but a complex control system is needed. The phase of the elements is controlled by varactors in this design, and the number of bias circuits is proportional

TABLE III
COMPARISON AMONG THE PROPOSED RECONFIGURABLE REFLECTARRAY

Reference	Reconfiguration method	Control unit number	Scanning range
[19]	Electrical	n	-47°~47°
[25]	Deformable ground (Mechanical)	4	-8°~8°
[26]	Rotatable reflectarray (Mechanical)	1	-60°~60°
[27]	Stretchable reflectarray (Mechanical)	1	35°~60°
Our Work	Drive mechanism (Mechanical)	1	-60°~60°

to the size of the reflectarray. Benteyn et al. [25] proposed a reflectarray with a deformable ground controlled by four motors, but the scanning range is narrow. By varying the tilt angle of the rotatable reflectarray, a wide scanning range is realized in [26]. However, when the beam is steered to 60°, a height variation of half the aperture length is demanded. A flexible concertina reflectarray achieves beam steering by adjusting the space of the subarray [27]. The reflectarray can be controlled by one motor, but the scanning range is in half of a plane from 35° to 60°. The proposed reflectarray shows a wide scanning range from $-60°$ to 60°. The elements are controlled by a drive mechanism that guarantees consistent phase steps between adjacent elements. A limited height variation of $\lambda/2$ is required. Only one motor is required to connect to the drive shaft and a periodic beam scanning process can be achieved. Furthermore, the mechanical structure and the antenna elements are easy to be implemented.

V. CONCLUSION

In this article, a mechanically reconfigurable reflectarray actuated by a single motor is investigated. All the elements are made of metal tubes and controlled by cams. A novel drive mechanism is proposed to achieve single motor control. The Archimedean spiral cam work in conjunction with the drive mechanism generates a continuing increasing phase step on the aperture. A prototype of ten elements is fabricated and measured. Simulated results show that a beam steering from $-60°$ to 60° can be achieved. The beam steering capability of the reflectarray is validated successfully steering the main beam to 30°, 40°, and 50°. A maximum improvement of 16 dB on the received signal is achieved in the blind area. The improvement on each point demonstrates the wide cover range of the reflectarray. This work offers a new solution to the design of mechanically reconfigurable reflectarrays.

REFERENCES

[1] L. Liu, J. Zhang, and C. Liu, "Capacity enhancement measurements of passive repeater for tri-polarized MIMO channel," in *Proc. Asia–Pacific Microw. Conf. (APMC)*, Dec. 2015, pp. 1–3.

[2] D. Ha, D. Choi, H. Kim, J. Kum, J. Lee, and Y. Lee, "Passive repeater for removal of blind spot in NLOS path for 5G fixed wireless access (FWA) system," in *Proc. IEEE Int. Symp. Antennas Propag. USNC/URSI Nat. Radio Sci. Meeting*, Jul. 2017, pp. 2049–2050.

[3] L. Li et al., "Novel broadband planar reflectarray with parasitic dipoles for wireless communication applications," *IEEE Antennas Wireless Propag. Lett.*, vol. 8, pp. 881–885, 2009.

[4] D. Wang, R. Gillard, and R. Loison, "A 60 GHz passive repeater array with endfire radiation based on metal groove unit-cells," in *Proc. 9th Eur. Conf. Antennas Propag. (EuCAP)*, Apr. 2015, pp. 1–4.

[5] D. Wang, R. Gillard, and R. Loison, "A 60 GHz passive repeater with endfire radiation using dielectric resonator antennas," in *Proc. IEEE Radio Wireless Symp. (RWS)*, Jan. 2014, pp. 31–33.

[6] D. Wang, R. Gillard, and R. Loison, "A notched dielectric resonator antenna unit-cell for 60 GHz passive repeater with endfire radiation," in *Proc. 8th Eur. Conf. Antennas Propag. (EuCAP)*, Apr. 2014, pp. 3167–3170.

[7] B. Kim, H. Kim, D. Choi, Y. Lee, W. Hong, and J. Park, "28 GHz propagation analysis for passive repeaters in NLOS channel environment," in *Proc. 9th Eur. Conf. Antennas Propag. (EuCAP)*, Apr. 2015, pp. 1–4.

[8] P. Callaghan, P. Young, and C. Gu, "Corner reflectarray for indoor wireless applications," in *Proc. Antennas Propag. Conf. (APC)*, Nov. 2019, pp. 1–5.

[9] Q. Chen, Q. Yuan, S.-W. Qu, and K. Sawaya, "Dual-antenna system composed of patch array and open-ended waveguide for eliminating blindness of wireless communications," *IEICE Electron. Exp.*, vol. 7, no. 9, pp. 647–651, May 2010.

[10] Q. Chen, S.-W. Qu, J. Li, L. Wang, Q. Yuan, and K. Sawaya, "Dual-antenna system composed of patch array and planar Yagi-Uda array," in *Proc. 5th Eur. Conf. Antennas Propag. (EUCAP)*, Apr. 2011, pp. 1023–1026.

[11] L. Wang, S.-W. Qu, J. Li, Q. Chen, Q. Yuan, and K. Sawaya, "Experimental investigation of MIMO performance using passive repeater in multipath environment," *IEEE Antennas Wireless Propag. Lett.*, vol. 10, pp. 752–755, 2011.

[12] X. Pan, F. Yang, S. Xu, and M. Li, "A 10 240-element reconfigurable reflectarray with fast steerable monopulse patterns," *IEEE Trans. Antennas Propag.*, vol. 69, no. 1, pp. 173–181, Jan. 2021.

[13] F. Wu, R. Lu, J. Wang, Z. H. Jiang, W. Hong, and K.-M. Luk, "A circularly polarized 1 bit electronically reconfigurable reflectarray based on electromagnetic element rotation," *IEEE Trans. Antennas Propag.*, vol. 69, no. 9, pp. 5585–5595, Sep. 2021.

[14] F. Wu, R. Lu, J. Wang, Z. H. Jiang, W. Hong, and K.-M. Luk, "Circularly polarized one-bit reconfigurable ME-dipole reflectarray at X-band," *IEEE Antennas Wireless Propag. Lett.*, vol. 21, no. 3, pp. 496–500, Mar. 2022.

[15] O. Bayraktar, O. A. Civi, and T. Akin, "Beam switching reflectarray monolithically integrated with RF MEMS switches," *IEEE Trans. Antennas Propag.*, vol. 60, no. 2, pp. 854–862, Feb. 2012.

[16] J. Perruisseau-Carrier and A. K. Skriverviky, "Monolithic MEMS-based reflectarray antenna cell digitally reconfigurable over a 360° phase range," *IEEE Antennas Wireless Propag. Lett.*, vol. 7, pp. 138–141, 2008.

[17] H. Rajagopalan, Y. Rahmat-Samii, and W. A. Imbriale, "RF MEMS actuated reconfigurable reflectarray patch-slot element," *IEEE Trans. Antennas Propag.*, vol. 56, no. 12, pp. 3689–3699, Dec. 2008.

[18] M. Riel and J.-J. Laurin, "Design of an electronically beam scanning reflectarray using aperture-coupled elements," *IEEE Trans. Antennas Propag.*, vol. 55, no. 5, pp. 1260–1266, May 2007.

[19] Q. Liang and B. K. Lau, "Beam reconfigurable reflective metasurface for indoor wireless communications," in *Proc. IEEE Int. Symp. Antennas Propag. USNC-URSI Radio Sci. Meeting (APS/URSI)*, Dec. 2021, pp. 1603–1604.

[20] W. Zhang, Y. Li, and Z. Zhang, "A reconfigurable reflectarray antenna with an 8 μm-thick layer of liquid crystal," *IEEE Trans. Antennas Propag.*, vol. 70, no. 4, pp. 2770–2778, Apr. 2022.

[21] X. Yang et al., "A broadband high-efficiency reconfigurable reflectarray antenna using mechanically rotational elements," *IEEE Trans. Antennas Propag.*, vol. 65, no. 8, pp. 3959–3966, Aug. 2017.

[22] X. Yang et al., "A mechanically reconfigurable reflectarray with slotted patches of tunable height," *IEEE Antennas Wireless Propag. Lett.*, vol. 17, no. 4, pp. 555–558, Apr. 2018.

[23] J. P. Gianvittorio and Y. Rahmat-Samii, "Reconfigurable patch antennas for steerable reflectarray applications," *IEEE Trans. Antennas Propag.*, vol. 54, no. 5, pp. 1388–1392, May 2006.

[24] G.-B. Wu, S.-W. Qu, S. Yang, and C. H. Chan, "Low-cost 1-D beam-steering reflectarray with ±70° scan coverage," *IEEE Trans. Antennas Propag.*, vol. 68, no. 6, pp. 5009–5014, Jun. 2020.

[25] C. Benteyn, R. Gillard, E. Fourn, G. Goussetis, H. Legay, and L. Datashvili, "A design methodology for reconfigurable reflectarrays with a deformable ground," in *Proc. 14th Eur. Conf. Antennas Propag. (EuCAP)*, Mar. 2020, pp. 1–5.

[26] M. I. Abbasi, M. H. Dahri, M. H. Jamaluddin, N. Seman, M. R. Kamarudin, and N. H. Sulaiman, "Millimeter wave beam steering reflectarray antenna based on mechanical rotation of array," *IEEE Access*, vol. 7, pp. 145685–145691, 2019.
[27] P. Callaghan, P. Giannakou, S. G. King, M. Shkunov, and P. R. Young, "Linearly polarized reconfigurable reflectarray surface," *IEEE Trans. Antennas Propag.*, vol. 69, no. 10, pp. 6480–6488, Oct. 2021.

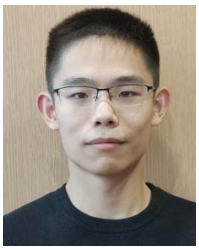

Zhongyao Cao received the B.S. degree from the University of Electronic Science and Technology of China, Chengdu, China, in 2020. He is currently pursuing the Ph.D. degree in electrical engineering with Tsinghua University, Beijing, China.

His current research interests include reconfigurable antennas, beam scanning arrays, and reflectarray antennas.

Yue Li (Senior Member, IEEE) received the B.S. degree in telecommunication engineering from Zhejiang University, Zhejiang, China, in 2007, and the Ph.D. degree in electronic engineering from Tsinghua University, Beijing, China, in 2012.

He is currently an Associate Professor with the Department of Electronic Engineering, Tsinghua University. In June 2012, he was a Post-Doctoral Fellow with the Department of Electronic Engineering, Tsinghua University. In December 2013, he was a Research Scholar with the Department of Electrical and Systems Engineering, University of Pennsylvania, Philadelphia, PA, USA. He was also a Visiting Scholar with the Institute for Infocomm Research (I^2R), A∗STAR, Singapore, in 2010, and Hawaii Center of Advanced Communication (HCAC), University of Hawaii at Manoa, Honolulu, HI, USA, in 2012. Since January 2016, he has been with Tsinghua University, where he is an Assistant Professor. He has authored and coauthored over 190 journal articles and 50 international conference papers and holds 25 granted Chinese patents. His current research interests include metamaterials, plasmonics, electromagnetics, nanocircuits, mobile and handset antennas, MIMO and diversity antennas, and millimeter-wave antennas and arrays.

Dr. Li was the recipient of the Issac Koga Gold Medal from URSI General Assembly in 2017; the Second Prize of Science and Technology Award of China Institute of Communications in 2017; the Young Scientist Awards from the conferences of PIERS 2019, ACES 2018, AT-RASC 2018, AP-RASC 2016, EMTS 2016, and URSI GASS 2014; the Best Paper Awards from the conferences of PIERS 2021, iWEM 2021, APCAP 2020/2017, UCMMT 2020, ISAP 2019, CSQRWC 2018, ISAPE 2021/2016, ICMMT 2020/2016, NCMMW 2018/2017, and NCANT 2019/2017; the Outstanding Doctoral Dissertation of Beijing Municipality in 2013; and the Principal Scholarship of Tsinghua University in 2011. He is serving as the Associate Editor of the IEEE TRANSACTIONS ON ANTENNAS AND PROPAGATION, IEEE ANTENNAS AND WIRELESS PROPAGATION LETTERS, *Microwave and Optical Technology Letters*, and Computer Applications in Engineering Education and also as the Editorial Board of Scientific Report, Sensors, and Electronics.

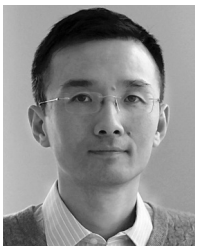

Zhijun Zhang (Fellow, IEEE) received the B.S. and M.S. degrees from the University of Electronic Science and Technology of China, Chengdu, China, in 1992 and 1995, respectively, and the Ph.D. degree from Tsinghua University, Beijing, China, in 1999.

In 1999, he was a Post-Doctoral Fellow with the Department of Electrical Engineering, The University of Utah, Salt Lake City, UT, USA, where he was appointed as a Research Assistant Professor in 2001. In May 2002, he was an Assistant Researcher with the University of Hawaii at Manoa, Honolulu, HI, USA. In November 2002, he joined Amphenol T&M Antennas, Vernon Hills, IL, as a Senior Staff Antenna Development Engineer and was then promoted to the position of Antenna Engineer Manager. In 2004, he joined Nokia Inc., San Diego, CA, USA, as a Senior Antenna Design Engineer. In 2006, he joined Apple Inc., Cupertino, CA, as a Senior Antenna Design Engineer and was then promoted to the position of Principal Antenna Engineer. Since August 2007, he has been with Tsinghua University, where he is a Professor with the Department of Electronic Engineering. He is the author of the book titled *Antenna Design for Mobile Devices* (Wiley, first edition, 2011; second edition, 2017).

Dr. Zhang served as an Associate Editor of the IEEE TRANSACTIONS ON ANTENNAS AND PROPAGATION (2010–2014) and the IEEE ANTENNAS AND WIRELESS PROPAGATION LETTERS (2009–2015).

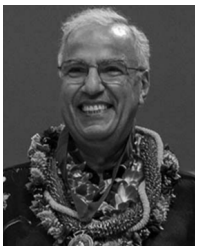

Magdy F. Iskander (Life Fellow, IEEE) was a Professor of electrical and computer engineering and the engineering clinic Endowed Chair Professor with the University of Utah, Salt Lake City, UT, USA. He joined the University of Hawaii at Manoa, Honolulu, HI, USA, in 2002, where he is currently a Professor of Electrical Engineering and the Director of the Hawaii Center for Advanced Communications, College of Engineering. He is also the Co-Director of the NSF Industry/University Cooperative Research Center with four other universities. He has authored over 250 articles in technical journals, holds nine patents, and has made numerous presentations at national/international conferences. He authored and edited several books, including the textbook *Electromagnetic Fields and Waves* (Prentice Hall, 1992, and Waveland Press, 2001; second edition 2012), and four books published by the Materials Research Society on Microwave Processing of Materials. His research in computational and biomedical electromagnetics and wireless communications was funded by the National Science Foundation, National Institute of Health, Army Research Office, U.S. Army CERDEC, Office of Naval Research, and several corporate sponsors.

Dr. Iskander was a recipient of many awards for excellence in research and teaching, including the University of Hawaii Board of Regents' Medal for Excellence in Research in 2013, the Board of Regents Medal for Teaching Excellence in 2010, and the Hi Chang Chai Outstanding Teaching Award in 2011 and 2014, which is based on votes by graduating seniors. He was also a recipient of the IEEE MTT-S Distinguished Educator Award in 2013, the IEEE AP-S Chen-To Tai Distinguished Educator Award in 2012, and the Richard R. Stoddard Award from the IEEE EMC Society in 1992. He received the Northrop Grumman Excellence in Teaching Award in 2010, the American Society for Engineering Education Curtis W. McGraw National Research Award in 1985, and the ASEE George Westinghouse National Award for Excellence in Education in 1991. He was the President of the IEEE Antennas and Propagation Society in 2002, a Distinguished Lecturer, and a Program Director of the Electrical, Communications, and Cyber Systems Division at the National Science Foundation. He has been the Founding Editor of the Computer Applications in Engineering Education Journal (Wiley), since 1992.